REPORT DOCUMENTATION PAGE

Form Approved OMB NO. 0704-0188

The public reporting burden for this collection of information is estimated to average 1 hour per response, including the time for reviewing instructions, searching existing data sources, gathering and maintaining the data needed, and completing and reviewing the collection of information. Send comments regarding this burden estimate or any other aspect of this collection of information, including suggesstions for reducing this burden, to Washington Headquarters Services, Directorate for Information Operations and Reports, 1215 Jefferson Davis Highway, Suite 1204, Arlington VA, 22202-4302. Respondents should be aware that notwithstanding any other provision of law, no person shall be subject to any oenalty for failing to comply with a collection of information if it does not display a currently valid OMB control number.
PLEASE DO NOT RETURN YOUR FORM TO THE ABOVE ADDRESS.

1. REPORT DATE (DD-MM-YYYY)	2. REPORT TYPE	3. DATES COVERED (From - To)
02-08-2023	Thesis or Dissertation	-

4. TITLE AND SUBTITLE	5a. CONTRACT NUMBER
HIGH-RESPONSIVITY SWIR ALLOY PHOTODETECTORS	W911NF-21-1-0129
	5b. GRANT NUMBER
	5c. PROGRAM ELEMENT NUMBER 611102
6. AUTHORS Henry Cain	5d. PROJECT NUMBER
	5e. TASK NUMBER
	5f. WORK UNIT NUMBER

7. PERFORMING ORGANIZATION NAMES AND ADDRESSES	8. PERFORMING ORGANIZATION REPORT NUMBER
Louisiana State University and A&M Colle[illegible] Office of Sponsored Programs 202 Himes Hall Baton Rouge, LA 70803 -0001	
9. SPONSORING/MONITORING AGENCY NAME(S) AND ADDRESS (ES)	10. SPONSOR/MONITOR'S ACRONYM(S) ARO
U.S. Army Research Office P.O. Box 12211 Research Triangle Park, NC 27709-2211	11. SPONSOR/MONITOR'S REPORT NUMBER(S) 78589-PE-II.3

12. DISTRIBUTION AVAILIBILITY STATEMENT

13. SUPPLEMENTARY NOTES

The views, opinions and/or findings contained in this report are those of the author(s) and should not contrued as an official Department of the Army position, policy or decision, unless so designated by other documentation.

14. ABSTRACT

15. SUBJECT TERMS

16. SECURITY CLASSIFICATION OF:			17. LIMITATION OF ABSTRACT	15. NUMBER OF PAGES	19a. NAME OF RESPONSIBLE PERSON
a. REPORT	b. ABSTRACT	c. THIS PAGE			Kevin McPeak
					19b. TELEPHONE NUMBER 225-578-0058

Standard Form 298 (Rev 8/98)
Prescribed by ANSI Std. Z39.18

REPORT DOCUMENTATION PAGE (SF298)
(Continuation Sheet)

Continuation for Block 13

Proposal/Report Number: 78589.3-PE-II

Report Title: HIGH-RESPONSIVITY SWIR ALLOY PHOTODETECTORS
Report Type: Ph.D. Dissertation

Publication Type: Thesis or Dissertation
Institution: Louisiana State University
Date Received: 02-Aug-2023 Completion Date: 12/1/21 10:48PM
Title: HIGH-RESPONSIVITY SWIR ALLOY PHOTODETECTORS
Authors: Henry Cain
Acknowledged Federal Support: **Y**

HIGH-RESPONSIVITY SWIR ALLOY PHOTODETECTORS

By

Henry W. Cain

Thesis Project
Submitted in Partial Fulfillment of the
Requirements for the Degree of

BACHELOR OF SCIENCE IN PHYSICS

Louisiana State University
December 2021

ABSTRACT

The SWIR light wavelength range is typically defined from 900 – 1700nm which is outside of the fairly minimal range humans can naturally view of visible light (350 – 700nm). SWIR photodetectors allow for the conversion of infrared light to visible light and have a plethora of applications in the modern world for visualization in fields such as surveillance, bioimaging, inspection, pollution, agriculture, automotive and many more. With SWIR photodetection being such a widely used technology, a demand for low-cost, ultra-high responsivity photodetectors sensitive to the SWIR wavelength range has surfaced. The most commonly utilized materials for SWIR detection lie in the III-V semiconductor family with InGaAs absorbers currently dominating the market. Although these materials' spectral photosensitivity is high within the relevant wavelength range, they are costly to manufacture and have limited response times as well as poor silicon device integration. A viable alternative could be utilizing a metal-silicon schottky barrier interface to extend silicon's detection range to the SWIR regime. This type of device utilizes a photoexcited metal to generate "hot" carriers as a means of converting incident photons into a measurable electrical charge. It is necessary that the metal have sufficient hot-carrier generation in the SWIR as well as a suitable carrier mean free path. Transition metals provide good absorption in the SWIR but have short carrier lifetimes due to their large electronic density of states near the Fermi level.

Alloys can offer emergent properties not available with pure metals [1]. Through the alloying of certain transition metals, the resulting metal's optical and electronic properties can be tuned via band hybridization to be a viable hot carrier generator. This work represents an ongoing effort in the goal to explore a new class of materials viable for ultra-fast current generation upon SWIR excitation.

TABLE OF CONTENTS

Chapter 1: Introduction and Background . . . 4

1.1 Alloys & Band Hybridization . . . 5

Chapter 2: Fabrication Methods . . . 7

2.1 Silicon Preparation . . . 7

2.1.1 KOH Etching . . . 7

2.1.2 Boron Doping . . . 7

2.2 Photolithography and Masking . . . 9

2.3 Depositional Methods . . . 10

2.4 TLM Method . . . 11

Chapter 3: Device Fabrication . . . 13

Chapter 4: Measurement Methods & Prospective Conclusions . . . 18

4.1 Characterization of Alloy . . . 18

4.2 Prospective Device Measurement & Goals . . . 18

References . . . 21

CHAPTER 1

INTRODUCTION AND BACKGROUND

Hot carrier generation is a promising route for creating SWIR photodetectors with fast rise times. Carriers can be difficult to collect as they can quickly recombine or thermalize with their surroundings soon after generation. A method to avoid such is to create a metal-semiconductor Schottky interface to collect the carriers. Alloys are often utilized due to their tunable dielectric function and thus optical properties. The metals must be able to generate sufficient hot carriers with suitable lifetimes upon SWIR light excitation. Mechanisms that allow for the generation of hot carriers include: *Landau damping*, *Interband* and *Intraband transitions* [2]. In this work, interband ($d \rightarrow sp$) electron transitions are utilized with an alloy engineered to have an abundance of d-state electrons as a means of generating a measurable current.

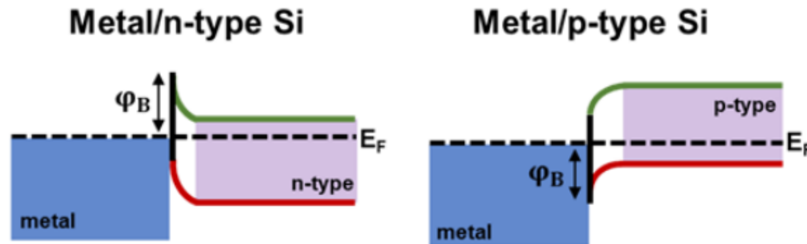

Figure 1.1: Schottky junctions for metal to n-type & p-type Silicon.

In this transition, an incident photon is absorbed and an excited electronic state is formed. Transitions must occur from occupied states below the Fermi level (valence band) to unoccupied states above it (conduction band) due to the Pauli Exclusion Principle [3]. In our metal alloy, these transitions are *direct* meaning crystal lattice momentum is conserved [4]. This sort of transition dominates when the excitation energy exceeds the interband threshold energy of the material. "Hotter" or higher energy holes than electrons are generated through this process by our alloy. If the hot-holes have sufficient energy to overcome the Schottky barrier, the holes will be injected

into the semiconductor and can be collected at a contact. To accept the high energy holes from the photoexcited metal, we utilize p-Si. A bias voltage is often applied across the Schottky junction, creating an electric field at the interface and improving carrier collection.

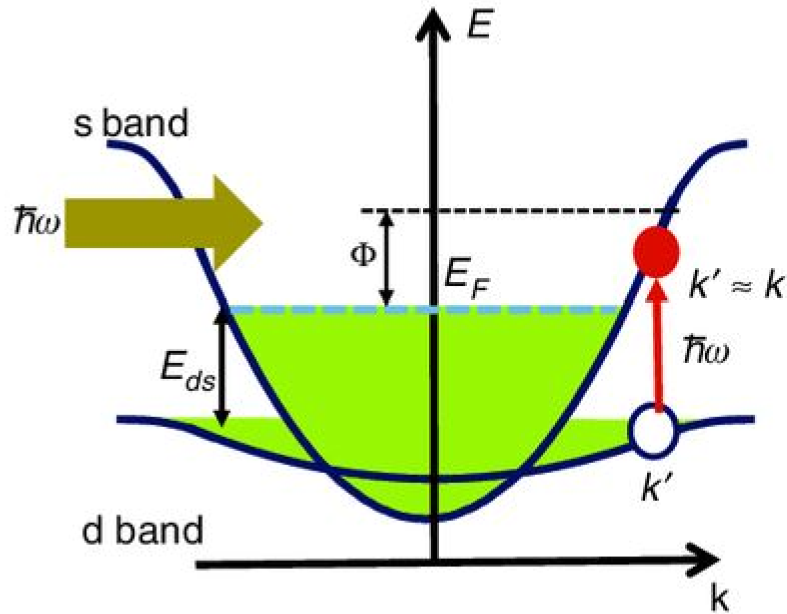

Figure 1.2: Direct interband transition process upon photoexcitation that creates a carrier energetic enough to surpass the threshold barrier Φ. Reprinted from ”Fundamental limits of hot carrier injection from metal in nanoplasmonics” by J. Khurgin, 2019, *Nanophotonics, 9*. Copyright 2019 De Gruyter.

1.1 Alloys & Band Hybridization

The optical properties of a material are directly related to its electronic density of states (EDOS) [5]. Noble metals have long been utilized to generate hot carriers through interband transitions [6] but SWIR photons do not have the energy required to surpass their interband energy threshold (IET). Alloys, however, can provide unique properties that are not reflected by its constituents. Alloying of certain metals can result in a shift of their EDOS [7]. By shifting the alloys EDOS closer to the Fermi level through alloying, hot carrier generation efficiency in the new metal under

SWIR photoexcitation would improve. Figure 1.3 demonstrates the useful properties that can be obtained through alloy exploration specifically between two noble transition metals. Gold has sufficient carrier lifetime but is unable to undergo interband transitions through SWIR stimulation as its EDOS is far from the Fermi level. Conversely, Palladium is able to have interband transitions but has poor carrier lifetime, quickly thermalizing with their environment. An alloy of these two metals in the form of Au_xPd_{1-x} has sufficient carrier lifetime in addition to the necessary band structure for interband transitions to occur.

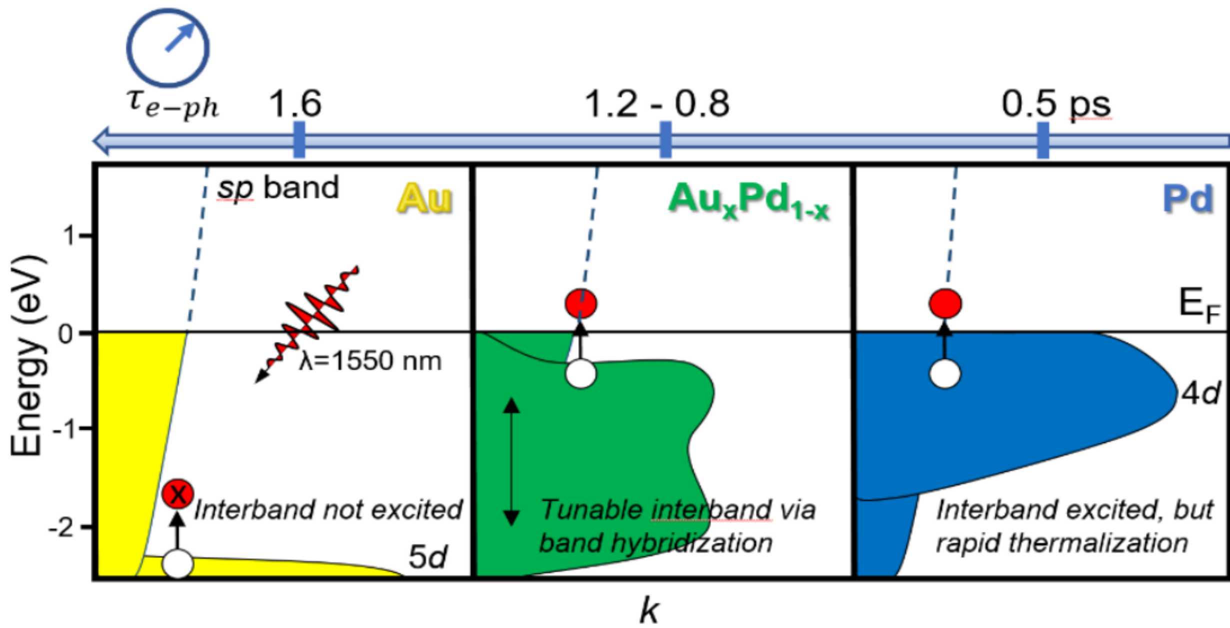

Figure 1.3: Alloying of AuPd showing tunable d-band position and carrier lifetime in the SWIR. Reprinted from "A Noble-Transition Alloy Excels at Hot-Carrier Generation in the Near Infrared" by S. Stofela, K. McPeak, 2020, *Advanced Materials, 32*. Copyright 2020 Wiley.

CHAPTER 2
FABRICATION METHODS

2.1 Silicon Preparation

2.1.1 KOH Etching

Surface texturing of crystalline silicon wafers is used in a variety of fields from the solar cell industry to MEMS (Microelectromechanical Systems) device fabrication. Aqueous Potassium Hydroxide (KOH) solution is often used to wet etch silicon and thus alter its surface topography. This etching process depends heavily on the temperature and concentration of the solution as well as the crystallographic plane of the silicon. Etch rates vary with differing crystallographic orientations due to the atomic bonds formed at the surface silicon atoms [8]. Isopropyl Alcohol (IPA) is commonly used in KOH wet-etching processes as an etch rate modulator. In this project, KOH etching is performed on (100) p-Si to produce a pyramidal surface topography. This pyramidal structure is desirable on the photodetector device as it greatly reduces the reflectivity of the surface across the entire infrared spectrum as it creates an impedance gradient. Light reflection at the surface is one of the main loss mechanisms in optoelectronic devices and KOH surface texturing is an often used tool to mitigate this. [9].

2.1.2 Boron Doping

Doping is the process of introducing impurities into a semiconductor's crystal lattice to modify its conductivity. Boron is a commonly used dopant for increasing silicon's conductivity as it has one less valence electron than silicon. Supplanting boron atoms in the silicon crystal lattice thus leaves a hole in the valence band of the silicon atoms affording more mobility to the valence electrons. Methods for doping include ion implantation and diffusion processes. In ion implantation, charged dopants are accelerated through an electric field and penetrate the surface of a substrate.

Penetration depth can be carefully tuned by adjusting the electric field strength.

The doping method utilized in this work is diffusion. Diffusion of boron atoms into a silicon substrate is typically accomplished through use of a spin-on dopant (SOD). In this process, a liquid boron solution is spincoated onto a substrate. The substrate is then placed into a diffusion furnace at very high temperatures (typically around 1000°C). Some of the silicon atoms in the crystal lattice are therefore able to gain enough energy to leave the lattice and are substitutionally replaced by boron atoms. Boron doping is used here to decrease contact resistance (R_c) as it increases the number of acceptors within the impure Si substrate as well as to create an ohmic metal-semiconductor interface for carrier collection. [10]. Contact resistance is characterized through the TLM Method (described in 2.4).

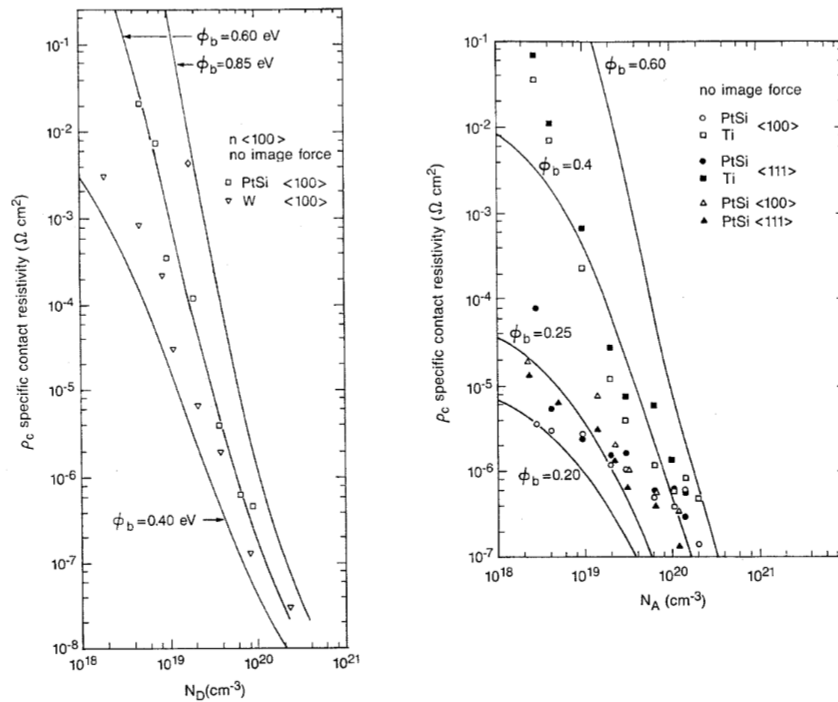

Figure 2.1: Specific contact resistivity of metal contacts to n-type & p-type Si. Reprinted from S. Swirhun, Electrochem. Soc., Oct. 1988.

2.2 Photolithography and Masking

Photolithography is widely used in microfabrication for patterning thin films or masking substrate regions for etching processes. A liquid photoresist (PR) is spun onto a substrate at the desired thickness according the manufacturer's spin curves and baked to harden. UV light is then used to expose certain regions of the PR covered substrate. The localized exposure process is accomplished through mask alignment, where a mask blocks the regions of the substrate one does not wish to expose. This can be done through physical masks or by direct writing with a virtual mask aligner. The substrate is them placed in an appropriate developer for the photoresist used. If the PR is *positive*, the exposed area will be removed during the development process. Conversely, the exposed region will remain post-development if a *negative* PR is utilized.

The resulting substrate composed of a patterned PR layer with exposed substrate regions can be used in a variety of ways. For example, the PR can act as a mask for anisotropic etching processes such as reactive ion etching (RIE). In RIE, a chemically reactive plasma is used to etch material off of a substrate. If a PR mask is in place and the desired plasma will not etch it, the plasma will only etch the exposed regions of a substrate allowing for a wide variety of fabrication capabilities. The PR is an organic and can be subsequently removed with an acetone dip. While this explains the role of PR masking in material removal, it is also frequently used in deposition processes. If material is deposited on the developed PR coated substrate using one of the depositional methods mentioned in 2.3, The deposited material will be overlying a PR layer everywhere except for the developed areas where ideally the material has good adhesion with the substrate surface. Acetone or other organic solvents such as n-methyl-2-pyrrolidone (NMP) can be used to perform a process called ”lift-off” to remove the PR layer as well as the overlying deposited material. These techniques are powerful tools that prove to be extremely useful in the creation of opto-electronic devices.

2.3 Depositional Methods

Thin film materials are the key elements of continued technological advances made in the fields of optoelectronic, photonic and magnetic devices [11]. There are many ways in which one can deposit thin films onto a substrate, but the relevant methods utilized here are electron beam (or E-beam) evaporation & magnetron sputtering. E-beam evaporation is a physical vapor deposition process (PVD) that takes place under high vacuum conditions where a target anode is bombarded with an electron beam created by a charged filament. The electron beam vaporizes atoms in the target material and precipitates solid atoms onto a mounted substrate. The deposition rate is monitored through the change in mass of an auxiliary quartz piezocrystal within the chamber. Depositional rates are often set by the deposited material's oxygen reactivity as highly reactive materials will oxidize in the transport process to the substrate [12] Feedback from the quartz piezocrystal is sent to the filament's power supply in an attempt to maintain a stable, set deposition rate. E-beam evaporation is utilized in this work for the deposition of the contacts designed to collect and transport the hot carriers.

In the sputtering PVD process, a chamber is pumped down to high pressure before a gas is introduced into the system. A large potential is generated by an RF or DC source between the target material and the chamber walls, ionizing the gas and accelerating electrons into the target. These collisions have sufficient energy to knock atoms off of the target and deposit them as a thin film on a mounted substrate. Magnetron sputtering adds high strength magnets to the target space to confine the electrons to a small region at the surface of the target, increasing plasma density as well as deposition rates as depicted in Figure 2.1. Magnetron sputtering has the benefit over other PVD processes of not requiring melting or evaporation of the target material, giving it the ability to deposit insulators as well as metals. If a sputterer has multiple targets and ways to generate the large potentials required, cosputtering becomes an option. By sputtering two separate targets at once and depositing at specific rates, it is possible to sputter a desirable alloy onto a substrate. In this project, the hot carrier generating AuPd thin film will be cosputtered onto p-Si.

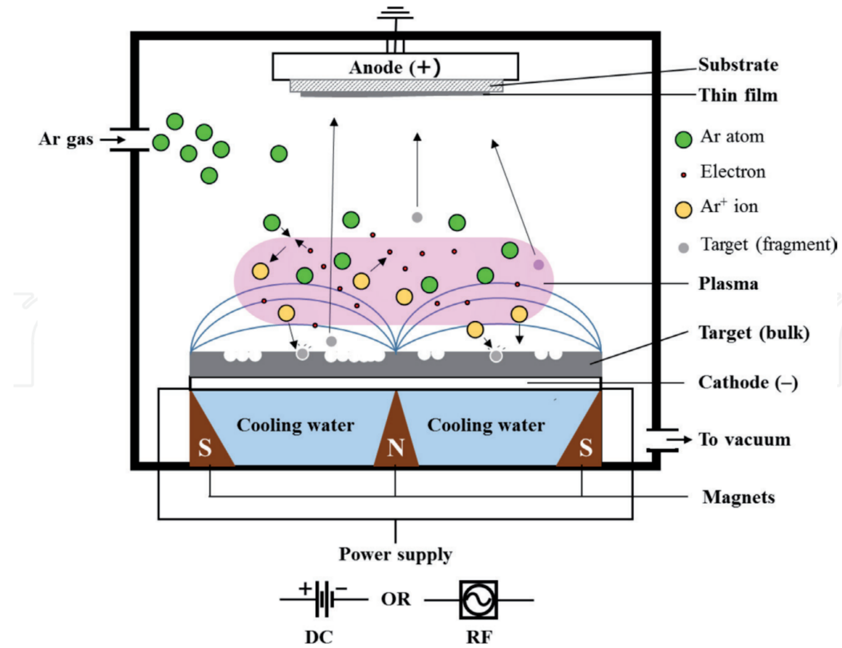

Figure 2.2: Magnetron sputtering process involving Argon as the ionized gas. Reprinted from ”Methods of Fabricating Thin Films for Energy Materials and Devices” by P. Hishimone, H. Nagai, M. Sato, 2018. Copyright 2020 IntechOpen.

2.4 TLM Method

In many opto-electronic devices, characteristics of the electrical contacts can have a significant impact on the performance of the device. An important factor to characterize when dealing with ohmic contacts is that of its contact resistivity. The transmission line model (TLM) is a commonly used tool to describe such a value. Contact resistivity can be described by:

$$\rho_c = R_c A_c = R_c L_T W \tag{2.1}$$

L_T is not the full length of the contact but rather a value called the ”transfer length”. The transfer length is the average distance an electron or hole travels beneath the contact before flowing into it. Current flow from the substrate into the contacts is not uniform. Most of the current making its way into the contact is doing so at the inner edge closest to the auxiliary contact being measured. Across

the contact is an exponential drop-off in current in an effect referred to as ”current crowding” [13]. By probing the resistance values between each adjacent contact and linearizing the measured resistances as a function of length, some useful values for calculating the contact resistivity can be found. The y-intercept of the linearization is $2R_c$ while the x-intercept is $-2L_T$. With contact width W being known, everything needed to calculate the contact resistance ρ_c has been found.

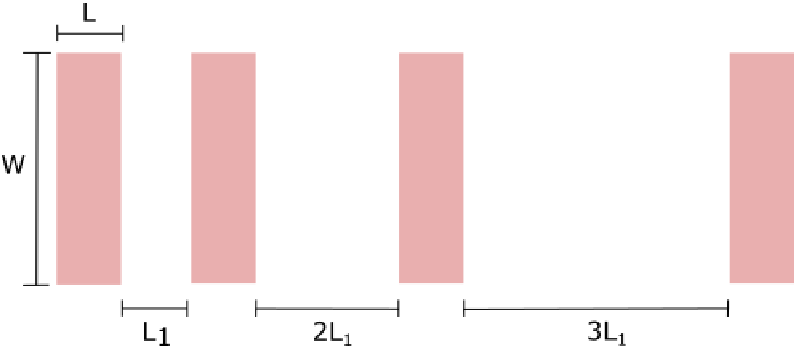

Figure 2.3: Contact layout in the TLM characterization process. Each identical contact is placed a further contact length apart from the previous contact separation distance.

CHAPTER 3

DEVICE FABRICATION

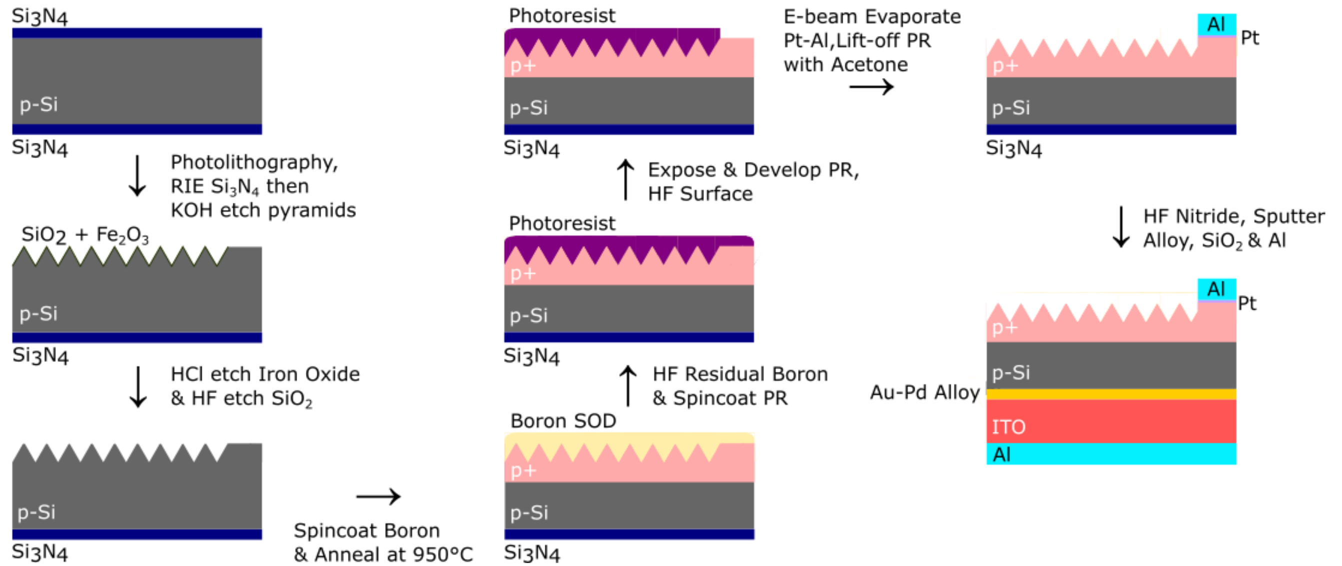

Figure 3.1: SWIR PD device fabrication flow chart.

We begin with (100) p-type, (1-10)Ω Si wafers that have been coated in 50nm of silicon nitride (Si_3N_4) as a means of protecting the back side of the wafer during the top-side fabrication process. Shipley S1813 PR is spun at 3000 rpm for 30s to give a thickness of about 1.6 microns according to the manufacturer's spin curves and confirmed by reflectometry. The substrate is subsequently baked at 115°C for 1 min to harden. The inner circles as well as fiduciary marks for alignment of the final device that can be seen in Figure 3.4 are exposed with an ML3 Microwriter virtual mask aligner. The substrates are left to develop in 4:1 DI water to 351 developer solution for 1 min before rinsing in DI water. It was found that residual photoresist would still remain in the exposed and developed regions. To resolve this issue, the substrate is placed in a Branson Plasma Asher with an oxygen plasma at 500W for 2 min.

Following photolithography, the substrates are placed in an Oxford Plasmalab 100 RIE with a CF4 plasma to etch away the exposed Si_3N_4. Prior to KOH surface texturing, the wafers are acetone-dipped to remove PR as well as covered in 10% HF on the light-incident side for 30s to remove the SiO_2 that formed during the high temperature conditions of the Si_3N_4 coating process. The substrates are then placed in a solution of 5%wt KOH, 3%wt IPA & 92%wt DI water with the Si_3N_4 protecting most of the surface. During evaluation of surface reflectivity in a Hitachu U-2001 spectrophotometer, this formula was found to drop the Si reflectivity in the IR from about 33% to around 10%, rivalling some of the best KOH etching results claimed as of yet [14].

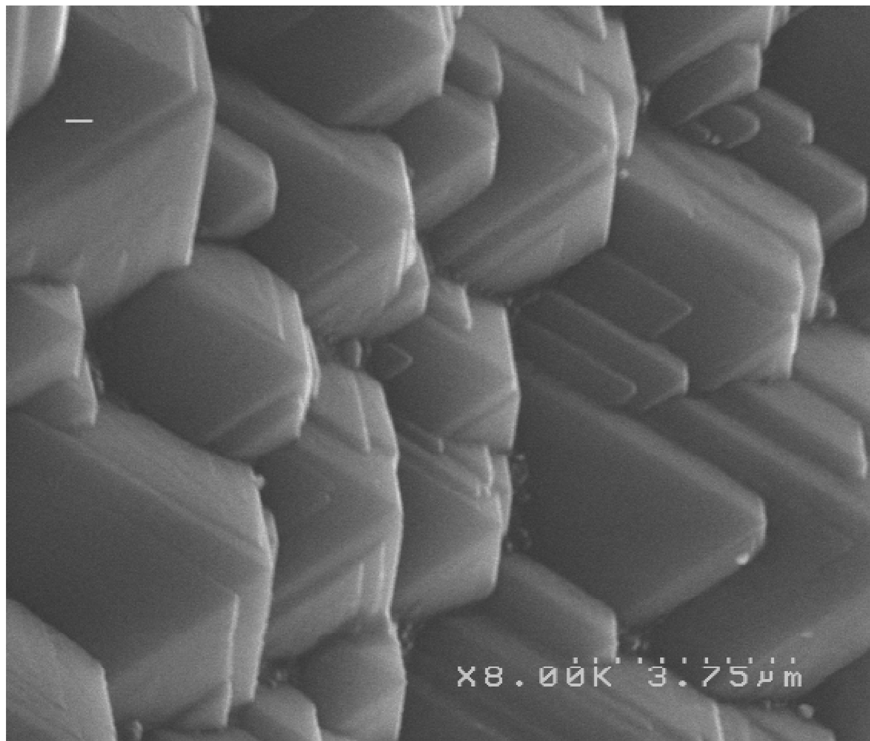

Figure 3.2: Angled SEM image of KOH etched Si surface.

Many profilometer scans of the surface topography revealed pyramid heights ranging from 2-6 microns in height. These results were the driver for the photolithography step previously described, allowing the carrier collection contacts to be deposited on a flat surface lest contact heights be greater than $6\mu m$ tall.

KOH contains trace Fe which forms iron oxide on the etched Si surface. The substrate was

submerged in a 5% HCl solution for 5 minutes to remove the iron oxide, followed by a single side 10% HF to remove the Si_3N_4 that was not removed in the ICP process. After 45min, the nitride is fully removed and the wafer is washed thoroughly with DI water in preparation for boron doping. HF on the Si surface was found to be forming H_2SiF_6, an issue resolved by the aforementioned rinsing. Any SiO_2 layer that may have formed during the rinsing stage is of no concern as the boron dopant is able to easily diffuse through it. Futurrex BDC1-2500 boron dopant is then spun onto the surface at 3000 rpm for 40s, allowed to dry then placed into a tube furnace at 400°C with 80 sccm drive-in process N_2 flow. The furnace is heated to 950°C for 30min and removed at 450°C. Through further doping of the top of the p-Si where the contacts will interface, ohmic contacts are able to form at the highly doped semiconductor-metal junction which will alloy carriers to be easily collected at them.

The quartz tube in the furnace used here has a max ramp rate of 5°C/min. In using a slow ramping furnace for the diffusion process, a surface roughness with frequent roughly 15nm deltas was observed. Boron dopant diffusion time was found to be correlated with surface roughness as seen in figure 3.3 [15]. Despite this, measurements of 7E-5 Ω/cm^2 for ρ_c were observed which is in line with Figure 2.1.

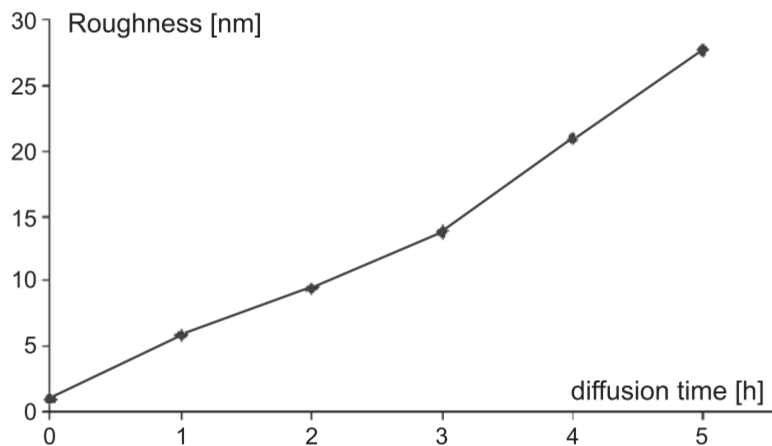

Figure 3.3: Roughness of silicon substrate surface post-boron diffusion. Reprinted from "Analysis of highly doping with boron from spin-on diffusing source" by C. Iliescu, M. Carp, J. Miao 2005, *Surface and Coatings Technology, 198.* Copyright 2005 Elsevier B.V..

Post-diffusion, the residual boron SOD forms a borosilicate glass and is removed by a 10% HF solution. Photolithography, following the previous steps through plasma ashing, is performed again, now with the exposed and developed region now being the contact rings and bonding areas as seen in Figure 3.4. The substrate is again subject to 10% HF and placed into an E-beam evaporator where 20nm Pt followed by 500nm Al are deposited at base pressures of 10^{-7} torr. Pt is deposited at a rate of 2nm/s while Al requires a significantly faster rate of 50nm/s to prevent mid-depositional oxidation due to its high reactivity. Acetone liftoff removes the PR and the unwanted PtAl film. The sample is then sintered at 320°C for 20min with forming gas flowing to prevent oxidation of the aluminum contacts. The thin layer of oxidation that forms when the Al comes out of the E-beam's vacuum chamber is easily punched through in a wire bonding or probing process of the ohmic contacts. Sintering the sample is shown to reduce contact resistivity further [16].

A common problem encountered in the use of aluminum contacts on silicon is the diffusion of Al into Si. This could be an issue here during the post-deposition sintering process as the highly doped silicon layer is only at the surface of the p-Si and Al could junction spike through it. The platinum barrier between the highly doped p-Si and Al significantly raises the breakdown temperature of the interface and prevents such from happening.

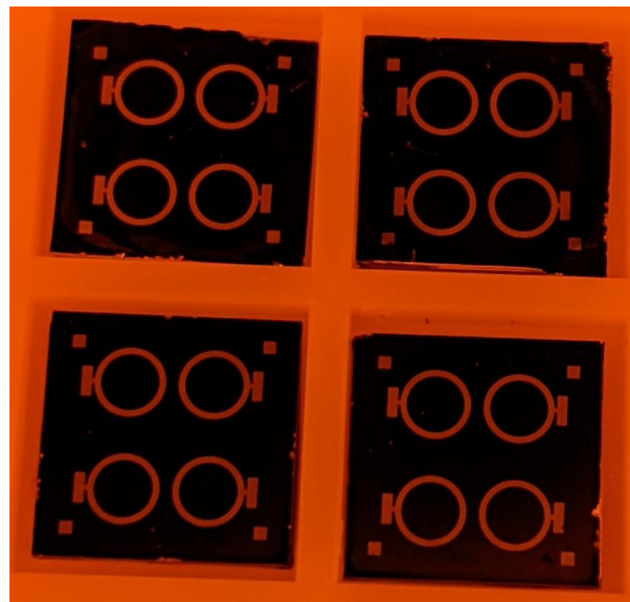

Figure 3.4: Top side of SWIR photodetector device.

To begin fabrication of the back-side of the substrate, the Si_3N_4 is wet etched with 10% HF. The sample is then placed in a KJL Dual Chamber Magnetron Sputterer with base pressures of 10^{-7} torr for deposition of the carrier generating alloy. A 10 nm Au_xPd_{1-x} alloy will be co-sputtered onto the substrate with Au on DC and PD on RF at yet to be determined rates. Without breaking vacuum, a layer of ITO will be directly deposited onto the alloy followed by a layer of Al. The ITO acts as a light trapping layer [17] with Al being a reflector to maximize the light-matter interactions that drive current generation in the device. The high conductivity of the ITO also enables the use of the aluminum reflector as the back-side ohmic contact. Each ohmic contact will be wire-bonded to a common pad or probed as a means of enabling carrier transport and therefore current measurements.

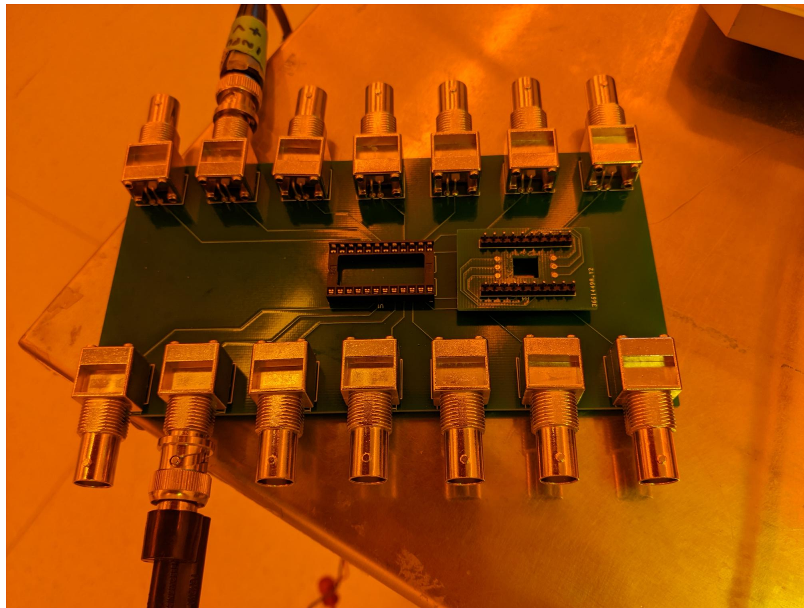

Figure 3.5: PCB enabling current measurements. Each device contact will be bonded to an Al pad on the top and bottom of the small PCB.

CHAPTER 4
MEASUREMENT METHODS & PROSPECTIVE CONCLUSIONS

4.1 Characterization of Alloy

To determine the alloy's band hybridization, angle-resolved photoemission spectroscopy (ARPES) will be utilized. ARPES is based on the photoelectric effect, where an electron is ejected from the surface of a photoexcited material. The emitted photoelectron's emission angles and kinetic energies are observed and will be used to determine the material's EDOS [18]. A Woollam RC2 variable-angle spectroscopic ellipsometer will be used to determine the optical properties of the alloy thin film. Knowledge of the optical properties of the film will is necessary for understanding the role inter-band electron transitions have on optical loss.

The carrier dynamics of the alloy film will be studied on insulating substrates post SWIR wavelength range pump by probing the temporal change in broadband THz transmission. An increase in terahertz transmission generally is consistent with a decrease in conductivity [19]. This change in conductivity is due to an increase in electron-phonon scattering as hot carriers thermalize with their surroundings resulting in higher lattice temperatures. The alloy will also be studied on p-Si to determine the hot-hole injection efficiency. Again, the device will be SWIR THz pump-probed and the transient differential THz transmittance will be observed, as seen in Figure 4.1. This signal only arises due to hot-carrier injection into the Si.

4.2 Prospective Device Measurement & Goals

Characterization of the device will involve measuring its reflectivity, responsivity and rise time. For reflectivity measurements, a StellarNet spectrometer will be used. Electrical measurements will be taken on the top and bottom Al contacts via probing. The top-side of the device will be illuminated at normal incidence by a SWIR laser photodiode. Photocurrent will be measured via modulation of

a laser source with a Zurich MFLI Lock-in amplifier which will also collect the output signal. An attempt will be made to link the optical and electronic properties of the alloy film to the measured reflectivity and responsivity of the device. The expected primary source of photocurrent generation is inter-band transitions due to the abundance of d-band electrons from band hybridization. The minimum measurable rise time using the MFLI is 35 ns as the maximum input bandwidth of its oscilloscope is 10 MHz. This rise time is in line with current InGaAs photodetectors previously mentioned and is faster than modern commercial Ge detectors. It is expected that measurements of the rise times of the hot-carrier devices are orders of magnitude faster (moving into the picosecond range) but further equipment such as a sampling oscilloscope would be required to explore this.

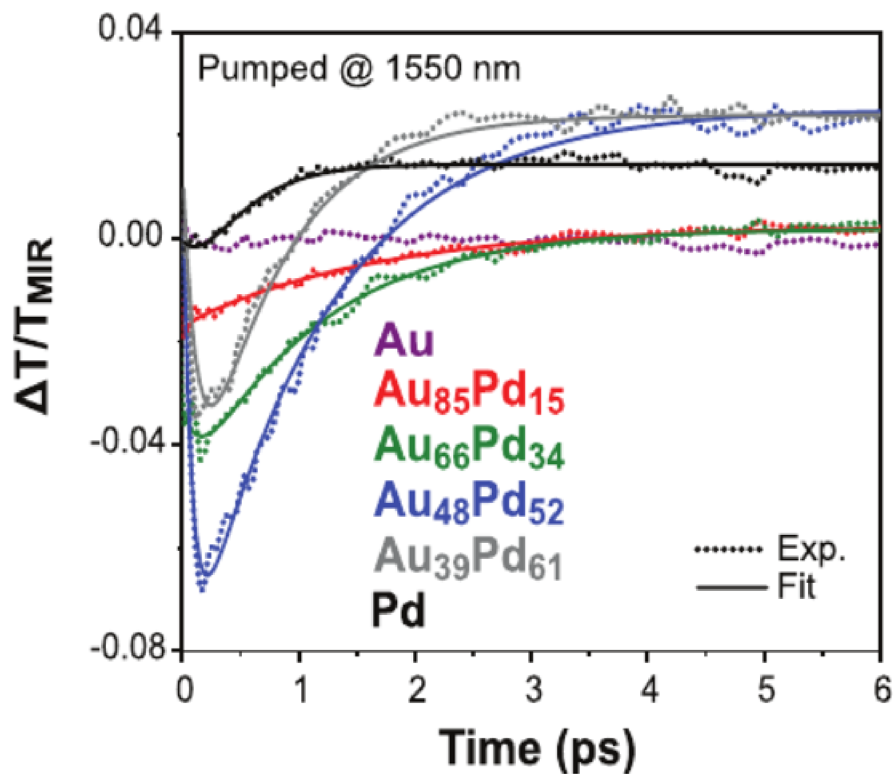

Figure 4.1: Temporal dependence of the transient differential transmittance, /T, for alloy films with 1550 nm pump and 3000 nm probe with experimental values (dotted) and two-temperature model fits (solid). Reprinted from ”A Noble-Transition Alloy Excels at Hot-Carrier Generation in the Near Infrared” by S. Stofela, K. McPeak, 2020, *Advanced Materials, 32*. Copyright 2020 Wiley.

REFERENCES

[1] M. Cortie and A. McDonagh, "Synthesis and optical properties of hybrid and alloy plasmonic nanoparticles," *Chem. Rev.*, vol. 111, pp. 3713–3735, 6 2011.

[2] J. Khurgin, "Hot carriers generated by plasmons: Where are they generated and where do they go from there?" *Faraday Discussions*, vol. 214, pp. 35–58, 2019.

[3] K. Kolwas and A. Derkachova, "Impact of the interband transitions in gold and silver on the dynamics of propagating and localized surface plasmons," *Nanomaterials*, vol. 10, p. 1411, 7 2020.

[4] M. Dresselhaus, *Solid State Physics Part II Optical Properties of Solids*. Springer, 2018.

[5] M. Cardona, "Optical properties and electronic density of states," *J. of res. of the NBS*, vol. 74(A), pp. 253–265, 2 1970.

[6] B. Cooper, H. Ehrenreich, and H. Philipp, "Optical properties of noble metals ii," *Phys. Rev.*, vol. 138, p. 494, 2A 1965.

[7] C. Langhammer, Z. Yuan, Z. Igor, and B. Kasemo, "Plasmonic properties of supported pt and pd nanostructures," *Nano Lett*, vol. 6, pp. 833–838, 4 2006.

[8] T. Monteiro, P. Kastytis, and S. Cardoso, "Dynamic wet etching of silicon through isopropanol alcohol evaporation," *Micromachines*, vol. 6, pp. 1534–1545, 10 2015.

[9] A. Husseini and B. Lahlouh, "Silicon pyramid structure as a reflectivity reduction mechanism," *Journal of Applied Sciences*, vol. 17, pp. 374–383, 8 2017.

[10] A. Scorzoni and M. Finetti, "Metal/semiconductor contact resistivity and its determination from contact resistance measurements," *Materials Science Reports*, vol. 3, pp. 79–137, 2 1988.

[11] M. C. Rao and M. S. Shekhawat, "A brief survey on basic properties of thin films for device application," *International Journal of Modern Physics*, vol. 22, pp. 576–582, 2013.

[12] K. McPeak, "Plasmonic films can easily be better: Rules and recipes," *ACS Photonics*, vol. 2, pp. 326–333, 3 2015.

[13] D. K. Schroder, *Semiconductor Material and Device Characterization*. John Wiley and Sons, 2006.

[14] S. Iqbal, L. Zhang, and X. Fu, “Highly-efficient low cost anisotropic wet etching of silicon wafers for solar cells application,” *AIP Advances*, vol. 8, 2 2018.

[15] C. Iliescu, M. Carp, and J. Miao, “Analysis of highly doping with boron from spin-on diffusing source,” *Surface and Coatings Technology*, vol. 198, pp. 309–313, 1-3 2005.

[16] M. Wittmer, “Barrier layers: Principles and applications in microelectronics,” *Journal of Vacuum Science Technology*, vol. A, p. 273, 2 1984.

[17] Y. Chao, F. Zhan, and H. Li, “Indium-tin-oxide nanorods for efficient light trapping in polymer solar cells,” *RSC Advances*, vol. 4, 58 2014.

[18] B. Lv, T. Qian, and H. Ding, “Angle-resolved photoemission spectroscopy and its application to topological materials,” *Nat Rev Phys*, vol. 1, pp. 609–626, 2019.

[19] K. Tielrooij, J. Song, and S. Jensen, “Photoexcitation cascade and multiple hot-carrier generation in graphene,” *Nature Phys*, vol. 9, pp. 248–252, 2013.